



Effect of tube material on convective heat transfer of various nanofluids

K. H. Solangi¹ · S. Sharif¹ · Bilal Nizamani²

Received: 9 May 2019 / Accepted: 13 September 2019 / Published online: 25 September 2019
© Akadémiai Kiadó, Budapest, Hungary 2019

Abstract

This work presents the convective heat transfer and friction loss characteristics of novel functionalized graphene-based and metal oxide nanofluids. The convective heat transfer in circular tubes of different materials (copper, aluminium and stainless steel 316) was used at constant wall heat flux of $23,870 \text{ W m}^{-2}$. An innovative approach was used to prepare highly dispersed propylene glycol-treated graphene nanoplatelets–water (GNP1) and trimethylolpropane tris amine–water (GNP2) by functionalization method. The measured thermal conductivity of GNP1 and GNP2 nanofluids showed incredible performance which increased up to 32% and 31% higher than that of basefluid. By comparing material effect, copper tube showed the highest HTC up to 119% in GNP1 at 0.1 mass%, while in aluminium and stainless steel 316 tube the highest heat transfer coefficient (HTC) was 110.2% and 100.68%. Besides, alumina and silicon dioxide nanofluids also presented decent increment in HTC which was up to 29.1% and 31.6%, respectively. The highest rise in friction factor for GNP1 and GNP2 was obtained up to 10.2% and 10%, respectively. For alumina and silicon dioxide nanofluids, the friction factor was measured up to 5.92% and 7.14% at velocity range of $1\text{--}3 \text{ m s}^{-1}$. The maximum enhancement in Nusselt number (Nu) for GNP, GNP2, alumina and silicon dioxide nanofluids was achieved up to 84%, 72%, 26% and 28%. The results suggest that the copper tube which is a good conductor of heat could be used in the heat exchangers and functionalized GNP nanofluids can be used as the heat exchanging fluids in heat transfer applications which could give a decent substitute to traditional working fluids in heat exchangers and in thermal fluid systems.

Keywords Nanofluids · Heat transfer · Copper · Aluminium · Stainless steel

List of symbols

D Diameter (m)
 L Tube length (m)
 C_p Specific heat ($\text{J kg}^{-1} \text{K}^{-1}$)
 Pe Peclet number
 V Velocity (m s^{-1})
 n Number of tubes
 q Heat transfer (W)

Nu Nusselt number
 m° Mass flow rate (kg s^{-1})
Re Reynolds number
 U Velocity (m s^{-1})
 T Temperature ($^{\circ}\text{C}$)
 W Pumping power
 k Thermal conductivity ($\text{W m}^{-1} \text{K}^{-1}$)
 H Heat transfer coefficient ($\text{W m}^{-2} \text{K}^{-1}$)
Pr Prandtl number
 A Area (m^2)
 F Friction factor

Electronic supplementary material The online version of this article (<https://doi.org/10.1007/s10973-019-08835-z>) contains supplementary material, which is available to authorized users.

✉ K. H. Solangi
solangi.quest@gmail.com

¹ School of Mechanical Engineering, Universiti Teknologi Malaysia, 81310 Johor Bahru, Johor, Malaysia

² Department of Electrical Engineering, Faculty of Engineering, University of Malaya, 50603 Kuala Lumpur, Malaysia

Greek symbols

ΔP Pressure drop (Pa)
 η Efficiency of loop
 ε Performance index
 μ Viscosity (Pa s)
 ρ Density (kg m^{-3})

Subscripts

w	Tube wall
p	Particles
nf	Nanofluid
bf	Basefluid
ID	Inner diameter
b	Bulkfluid
out	Outlet
OD	Outer diameter
Tb	Bulk temperature
in	Inlet

Introduction

Enhancement in heat transfer has been the attention of engineers not just for designing high productive and efficient systems, but also for satisfaction of safe operability of devices and systems. Highly improved properties by using advanced materials and techniques in heat transfer are highly demanded [1–5]. Since last few decades, a variety of conventional fluids like oil, ethylene glycol, water and air are already used for the transfer of heat depending on the area of applications [6, 7]. Similarly, several types of nanomaterials such as carbon nanotube (CNT), metal oxide, ceramic nitride and carbides are used in combination with conventional fluids to yield amazing heat conductors [8–12]. However, these nanofluids are affected by a number of factors which include nanomaterial size, viscosity, Brownian motion, interfacial nanomaterial layering and stability [13–15]. However, the performance of heat transfer fluids still turns out to be highly demanded and challenging where massive amount of heat is to be transferred. Further, several methods have been used to enhance the heat transfer in microchannel heat exchangers [16–19]. However, nowadays researchers have focused on the single-phase and two-phase heat transfer methods. Betz and Attinger [20] examined the intermediate step between single-phase flow and two-phase flow. They observed that segmented flow in microchannel heat sink enhances heat transfer up to 140% compared to the single-phase flow. However, this method has a limit of growing the instability and pressure drop inside the channel. Nowadays, graphene has been one of the newest topics in scientific community owing to its unique heat transfer, electronic and mechanical properties [11, 21–23]. Surely the graphene is an outstanding nanomaterial having thermal conductivity (TC) higher than other carbon-based nanomaterials, in the range between $4.84 \pm 0.44 \times 10^3$ and $5.30 \pm 0.48 \times 10^3 \text{ W m}^{-1} \text{ K}^{-1}$ [24, 25].

Sarafraz and Safaei [26] used the GNP nanofluids to study the thermal performance and efficiency of an evacuated solar collector. They achieved the enhancement in thermal conductivity up to 19% at 0.1 mass%. Further, they obtained the efficiency of the solar thermal collector which reached 95% by using GNP nanofluids at 0.1 mass% at a flow rate of 3 L min^{-1} . Hafiz and Waqas [8] used the GNP nanofluids to examine the angle effect of a pin fin heat sink channel in the convective heat transfer coefficient. They obtained the higher HTC with the decrease in the pin fin channel angle from 90 degrees to 22.5 degree. However, the convective heat transfer corresponding to 22.5- and 45-degree heat sink was 84.3% and 38.5% higher as compared to 90-degree heat sink, respectively. Sarafraz et al. [27] examined the heat transfer performance and thermophysical properties of nanofluids by using the aqueous GNP at concentrations of 0.025–0.1 mass%. A significant enhancement in heat transfer coefficient and Nusselt number was achieved up to 80%. However, they could observe that the enhancement in thermal performance was attributed to the thermophoresis effect, Brownian motion and higher thermal conductivity of the nanofluid.

It has been reported by several researchers that mostly the thermal conductivity (TC) of the carbon particles like graphene nanoplatelets (GNPs) and carbon nanotubes (CNTs) is high as compared to metal oxide or metal nanoparticles [24, 27–31]. This recent research proves that the carbon-based nanoparticles have high potential for increasing the thermophysical properties of basefluids [10, 32]. Nevertheless, in the field of nanofluids, the significant thermal properties of GNPs such as the strong van der Waals interactions, which have limited use in thermal applications. However, to overcome on this problem the covalent and non-covalent functionalization techniques are an effective approach to improve the dispersibility and increase the thermal properties of GNPs [33–36]. Hafiz and Waqas [8] examined the convective HTC of GNPs to investigate the angle effect of the pin fin heat sink channel. They measured the HTC for 22.5° heat sink which was 84.30% higher as compared to 90° heat sink. Sarafraz et al. [21] studied the convective single-phase heat transfer of GNP nanoparticles which were dispersed in water–ethylene glycol. However, they achieved the significant enhancement in thermal conductivity of GNP nanofluids up to 32.1% at 0.3 mass% and at 60 °C. Further, they observed the increase in thermal performance up to 21% in spite of a 12.1% augmentation in the pressure drop. Emad et al. [11] prepared the aqueous suspension of stable homogeneous GNP nanofluids by high-power ultra-sonication. In their experiment, they used the stainless steel 316 tube of 1400 mm in length with inner and outer diameters of 10 mm and 14 mm, respectively. They measured the Nu

(Nu) of GNP nanofluid which was nearly 83% higher than the basefluid, and the increase in pressure drop was up to 14.6%. In another study, Amiri et al. [5] examined the heat transfer characteristics of ethylene glycol-treated GNP-based water–ethylene glycol coolants over a backward-facing step. They used the functionalization technique to produce the ethylene glycol-graphene nanoplatelets (EGGNP) and EGGNP-based water–EG coolant (EGGNP-WEG). In their results, they observed a greater mass concentration of EGGNP in basefluid which indicated a higher extent of convective HTC and TC, suggesting high heat transfer rate over the backward-facing step. Arzani et al. [37] prepared the covalent and non-covalent functionalized GNPs, where they investigated the HTC for the convective heat transfer. High increment in transfer of heat was found in covalently functionalized GNPs up to 22% at 0.1 mass% due to their higher TC. It is well known that the two-phase flow provides the higher heat transfer rates compared to the single-phase flow, particularly in microchannel [38–41]. Therefore, the two-phase flow in microchannel heat exchangers with nanofluids is appropriate for convective heat transfer.

Numerous studies have focused on metal oxide nanofluids in heat exchangers [19, 25, 42, 43]. Tiwari examined the convective HTC of alumina and silicon dioxide water-based nanofluids by optimizing the various concentrations. The maximum HTC increments for alumina and silicon dioxide water-based nanofluids at 3 vol% were about 26.3% and 13.9% [44]. Bin et al. [45] inspected the HTC of alumina water-based nanofluids by using sodium dodecyl benzene sulfonate (SDBS) as dispersant. The enhancement in HTC was achieved up to 14.24% at 0.1 mass%. Moreover, oxide-based nanofluids have the better stability compared with other nanofluids [35]. Among the above examples, alumina and silicon dioxide have good thermal performance characteristics. Therefore, in this research from metal oxides alumina and silicon dioxide nanoparticles were chosen to prepare the nanofluids.

Abundant research has been done on GNPs and metal oxides as a coolant in the heat exchangers, where some researchers have used the copper or stainless steel as the test section material. As per authors' knowledge, no one has compared the materials effect of tube in the convective heat transfer by using GNPs and metal oxides nanofluids. Therefore, in this research different tubes with different material selections were used to investigate the increment in convective HTC and the pressure loss by the use of functionalized GNP water-based nanofluids. This research has focused on heat transfer characteristics and friction loss of propylene glycol-treated graphene nanoplatelets (GNP1), trimethylolpropane tris [poly (propylene glycol), amine terminated] ether-treated graphene nanoplatelets (GNP2), alumina and silicon dioxide water-based

nanofluids. The pristine graphene with the higher surface area being $750 \text{ m}^2 \text{ g}^{-1}$ was selected for functionalization with PG and TMP. The heat flux for the convective heat transfer in circular tubes of different materials was considered at $23,870 \text{ W m}^{-2}$, and the Reynolds number range was kept between 3900 and 11,700. All the experiments were conducted in closed conduit (pipe) flow. Further, the effect of the dispersed nanoparticle concentration on thermal properties, friction factor, Nu and convective HTC was thoroughly investigated. The objective of this work is to investigate the thermophysical properties of the developed nanofluids and their characterization and to examine the material effect on the transfer of heat performance of a circular tube heat exchanger in different tube materials.

Material and methodology

Materials preparations and selected functionalization approach for GNP1, GNP2, alumina and silicon dioxide nanofluids

For this research, pristine graphene nanoplatelets were purchased from XG sciences with $750 \text{ m}^2 \text{ g}^{-1}$ surface area and over 95% of carbon purity. The rest of all other chemicals and materials which were required for this study were purchased from Sigma-Aldrich.

For the preparation of GNP1, firstly, GNP was covalently functionalized with carboxyl groups. After the functionalization, pristine GNP was ultra-sonicated with the mixture of sulphuric acid and nitric acid in the volume ratio of 3:1 for up to 12 h at $60 \text{ }^\circ\text{C}$. After sonication, the mixture was stirred for 36 h at similar conditions to synthesize carboxylated GNP (GNP-COOH). To separate the suspension and supernatant to reach PH value around 4–5, further suspension was processed to centrifuge at 11,000 rpm with distilled water. Further to dry the sample, the suspension was kept in oven at $50 \text{ }^\circ\text{C}$ for 48 h. Also, in this work, 1 g GNP-COOH and 100 mL propylene glycol (PG) were sonicated for 10 min and after that 13.4 mL sulphuric acid was added in the suspension drop-by-drop. Further, the mixture was sonicated again for 8 h and then kept over a magnetic stirrer for 12 h at $70 \text{ }^\circ\text{C}$. Moreover, to surge the reaction rate and based on the equilibrium law, the produced water in Fischer esterification reaction was removed by evaporating water. During this process, the equilibrium was affected by either removing water product from the reaction mixture and it shifted to right side. However, the acid-catalysed esterification of carboxylic acids with alcohols can give an ester. Ultimately, to remove the non-reacted materials from the suspension, the mixture was centrifuged again at 11,000 rpm with anhydrous THF and was then rinsed a few times with THF and ethanol.

Finally, the sample was then kept in the oven at 60 °C for 48 h.

Similarly, for the preparation of GNP2 the method is same as for GNP1; in the GNP2 case after centrifugation when the pH reaches around 3–4, the sample is then kept in the oven, for around 4 days at 50 °C to dry overnight. Therefore, in the typical experiment 1 g GNP-COOH and, instead of propylene glycol, 100 mL of trimethylolpropane tris [poly (propylene glycol), amine terminated] ether were sonicated for 10 min and then 13.4 mL H₂SO₄ was added drop-by-drop. For the preparation of metal oxides nanofluids (alumina nanopowder with particle size of about 50 nm and silicon dioxide nanopowder with particle size of about 50 nm), a two-step method was used. Finally, to achieve the homogenous distribution of nanoparticles the sample was sonicated up to 60 min in order to break down the large agglomerates.

Experimental system

For this research, the conduit flow experimental set-up was designed and built as shown in Fig. 1a, which consisted of all required equipped parts and devices to conduct the experiment and analyse the data. The all components of the test rig and procedure are given in detail in supplementary information. Furthermore, for investigating material effect, the tubes were selected of same diameters with different materials (stainless steel, aluminium and copper). However, all the selected tube materials have different mechanical and thermal properties. The thermal conductivity of the stainless steel material is 16.2 W m⁻¹ K⁻¹, which is lower than that of both other selected materials. Further, metals like aluminium are good conductors of heat and they absorb heat very quickly. However, the thermal conductivity of aluminium is 205 W m⁻¹ K⁻¹. Also, our third selected test section material is copper which is the best conductor of heat in all selected materials. Nevertheless, the thermal conductivity of copper is 385 W m⁻¹ K⁻¹. Therefore, for material effect comparison the diameter of the test section tube was selected to be 4 mm. Figure 1b shows the three different tubes of the same diameter with different materials.

The thermophysical properties of selected nanofluids were measured at 0.1 mass% for this experiment and are given in Table 1. The TC of all samples was measured by the thermal properties analyser (KD2 pro), and this technique is used with transient hot wire method. Figure 1c presents the TC plot of GNP2, GNP1, silicon dioxide and alumina nanofluids which is the function of temperature and mass percentage. It is observed that the increase in the TC with temperature is more sensible in GNP2 and GNP1. Therefore, it assures that the temperature plays a vital role in growing the TC of both the coolants.

Results and discussion

Functionalization analysis of GNP1 and GNP2

Surface amendment of GNP by functional groups becomes significant in order to achieve the highly stable nanofluids. Figure 2a describes the Fourier-transform infrared spectroscopy (FTIR) spectra of pristine GNP and GNP1. Noticeably, the GNP1 sample proves clear cues of different functionality groups in difference to the original GNP. As in Fig. 2a, the spectrum of GNP1 gives the peaks at 1134 cm⁻¹ and 1642 cm⁻¹, which could be attributed to the C–O and C=O extending vibration. Likewise, another sharp peak at 1042 cm⁻¹ which is attributable to C–O stretching vibration of ester band, in result of the esterification of carboxylic acid groups on main structure or edge of GNP with –OH band of PG. Therefore, the confirmation of PG functionalization was done by observing peaks at 1453 cm⁻¹, 3403 cm⁻¹ and 1385 cm⁻¹ for the O–H, COO⁻ stretching vibrations and CH₂ bending vibration, respectively. However, the peaks observed at 2974 cm⁻¹ and 2931 cm⁻¹ agree with the stretching vibration of C–H groups. Similarly, Raman spectroscopy is a powerful technique for the investigation of the structural properties of carbon compounds [36]. Raman spectral analyses of the pristine GNP and GNP1 are presented in Fig. 2b which clearly describes that the both samples exhibit G and D bands, at about 1362 cm⁻¹ and 1592 cm⁻¹, respectively. The G bands relate to graphitic carbon (sp²), and the D bands are related to amorphous/disordered carbon (sp³). Because of covalent functionalization, the increase in ratio of I_D/I_G refers to the change of sp²-hybridized carbons to sp³-hybridized carbons. However, the dramatic increase in D band intensity is interpreted as the presence of faults and ailment shaped in the sample after dynamic mechanical and chemical process of acid treatment. However, it can be observed that intensity ratio of GNP1 sample is greater than the intensity of original GNP.

Figure 3 demonstrates images of pristine GNP and GNP1 which were taken by scanning electron microscopy (SEM) and transmission electron microscopy (TEM). Although TEM and SEM images cannot clearly differentiate minute functional groups, it can still show wrinkles and surface deterioration of GNPs that were formed due to PG functionalization. In general, some multi-layer GNP flakes with suitable grain size in images could be seen. However, as per the TEM and SEM images, the their size and shape of GNP1 samples were kept. In Fig. 3, in the SEM and TEM images the noticeable changes in surface deterioration and morphology can be clearly seen. In TEM images specifically, the lines observed are wrinkles on the GNP surface because of inherent instability of 2D

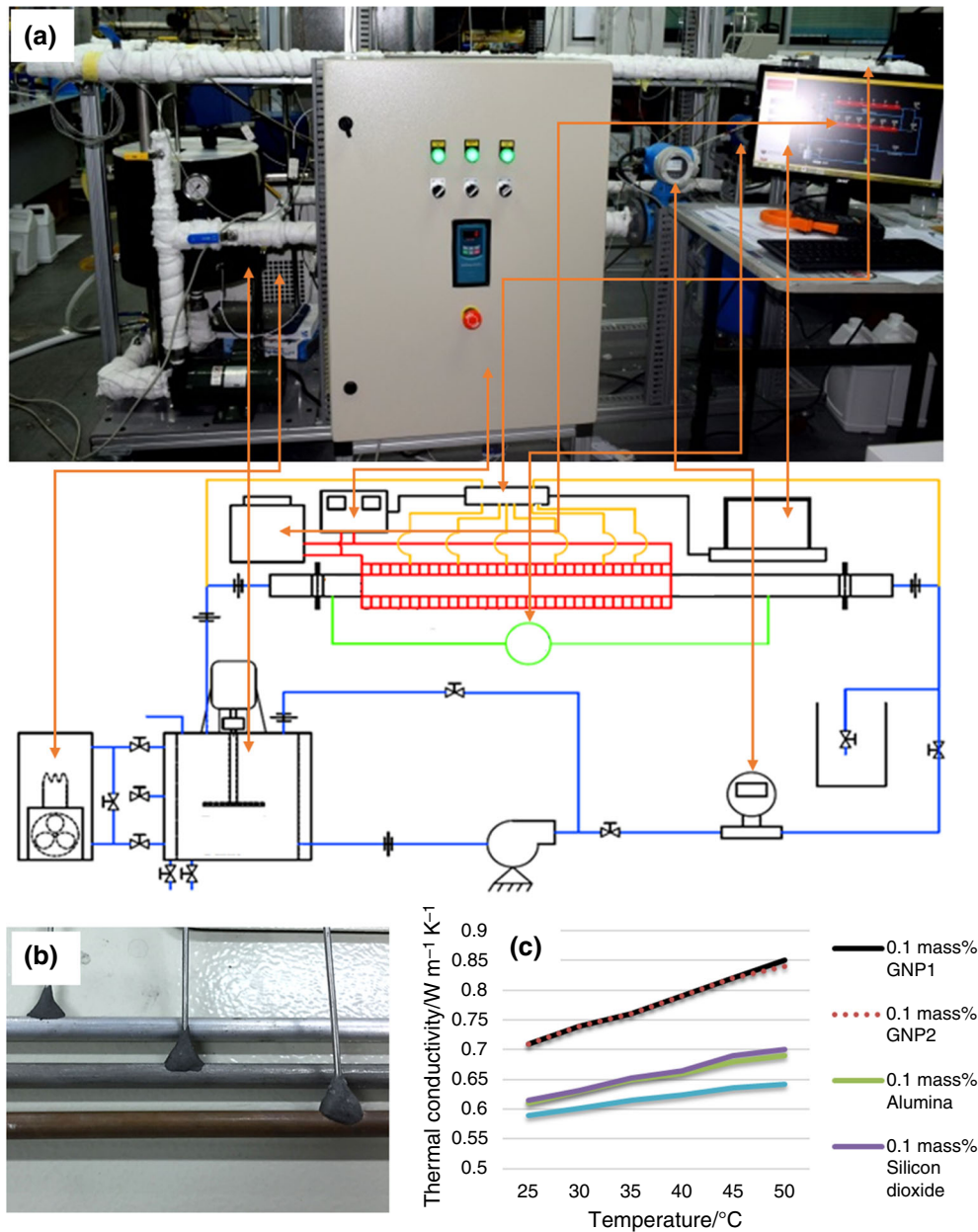


Fig. 1 a The designed and fabricated experimental set-up for measuring the convective heat transfer [29], b different test section tubes of the same diameter 4 mm (copper, aluminium and stainless steel), c variation of TC at different temperatures (°C)

Table 1 Viscosity, density and specific heat of the selected nanofluids

	Viscosity/Pa s	Density/kg m ⁻³	Specific heat/J kg ⁻¹ K ⁻¹
GNP1	0.003129	1055.863	2807.352
GNP2	0.003130	1055.863	2807.352
Alumina	0.002155	1072.747	3039.524
Silicon dioxide	0.003001	1057.886	2796.342

structures. However, in GNP1 the visible lines can be attributed to the augmentation of wrinkles (crinkliness) in the ultra-sonication process, which result from the flexibility of GNP flakes after the functionalization [29].

Figure 4a represents FTIR spectra of pristine GNP and GNP2. As it can be seen in the figure clearly, in difference to the pristine GNP, the GNP2 sample shows clear signs of various functionalities sets. However, Table 2 gives the

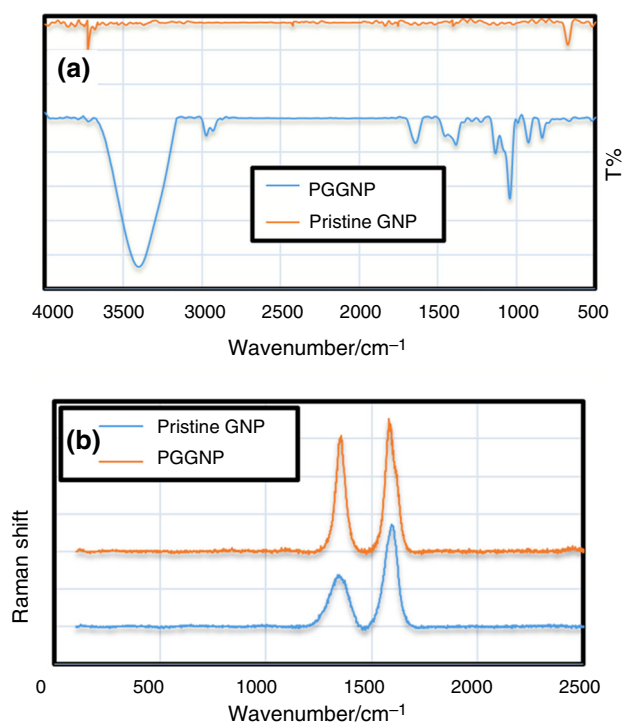


Fig. 2 **a** FTIR spectra of GNP1 and pristine GNP, **b** Raman spectra of GNP1 and pristine GNP [29]

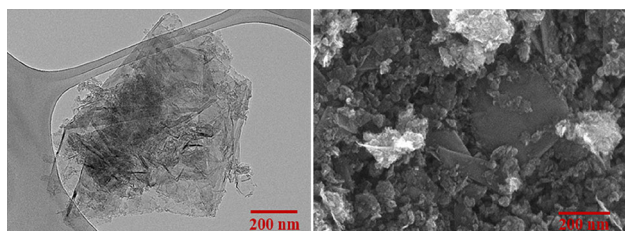


Fig. 3 TEM (at left) and SEM (at right) images of GNP1 at 0.1 mass%

peaks along with the explanation of their understandings. The spectrum of GNP2 shows few peaks at 1105 cm^{-1} and 1637 cm^{-1} , that can be attributed to C–O and C=O stretching vibration. These bonds are present due to the attachment of TMP molecules on the edge and surface of the GNP sheets. Further, at 919 cm^{-1} another small peak is observed which is attributable to C–O stretching vibration of ester band resulting from esterification of carboxylic acid groups on edge or the main structure of GNP with –OH band of TMP. Therefore, TMP functionalization is confirmed by the presence of peaks at 3430 cm^{-1} for N–H and O–H stretching vibration of symmetrical/primary amine –NH stretching vibration. Likewise, the peaks at 2876 cm^{-1} and 2968 cm^{-1} are in agreement with stretching vibration of C–H groups. Similarly, peak centred around 1575 cm^{-1} is attributable to the C=C stretching vibration as a result of the devastation of the main structure

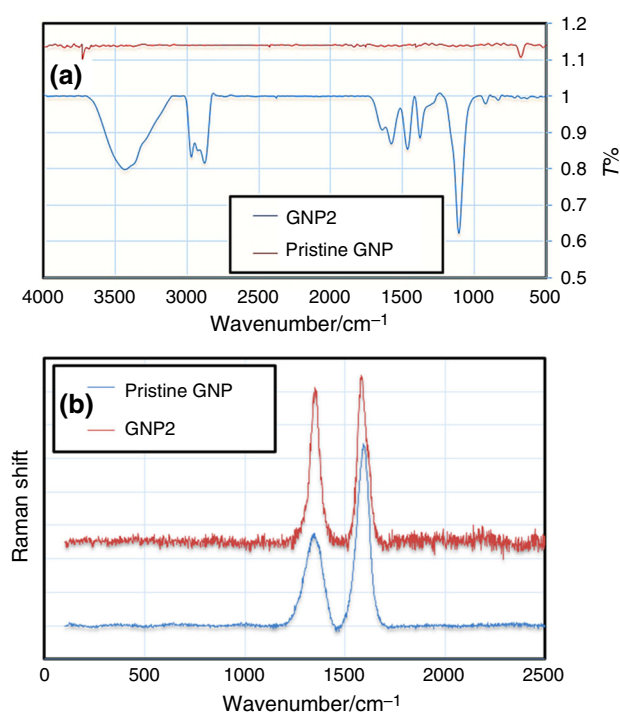


Fig. 4 **a** FTIR spectra of GNP2 and pristine GNP, **b** Raman spectra of GNP2 and pristine GNP [18]

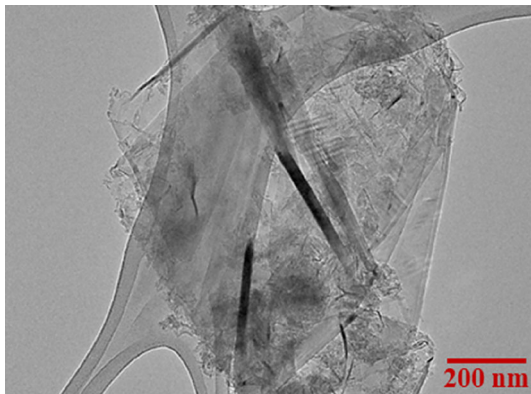
or open ends of GNP. TMP functionalization was further developed by the presence of peaks at 1375 cm^{-1} and 1463 cm^{-1} for the CH₂ and NH₂ bending vibrations, respectively. The appearance of these peaks in the FTIR spectrum for the GNP2 qualitatively proves the success of the covalent functionalization procedure.

In Fig. 4b, Raman spectral analysis of the pristine GNP and GNP2 is shown. The Raman spectroscopy of both pristine GNP and GNP2 samples reveals the G and D bands at around 1362 cm^{-1} and 1592 cm^{-1} , respectively. The D bands are attributed to the disordered/amorphous carbon (sp^3), and G bands are attributed to the graphitic carbon (sp^2). Because of covalent functionalization, the increase in ratio of I_D/I_G refers to the change of sp^2 -hybridized carbons to sp^3 -hybridized carbons. However, it is obvious that intensity ratio of GNP2 sample is surely higher than that of the pristine GNP. It could be noticed that the GNP2 and pristine GNP showed the I_D/I_G ratio of 0.92 and 0.51, which have an agreement with FTIR results.

The TEM image of GNP2 is shown in Fig. 5. It could be seen that the image shows wrinkles and the surface deterioration of GNPs that were formed as the result of GNP2 functionalization. In general, the GNP sheets with the large grain size in image can be clearly seen. Besides, the lines seen in this image are wrinkles on the GNP surface due to the inherent instability of 2D structures. The appearance of these lines in GNP2 can be attributed to the improvement in wrinkles (waviness) during the sonication procedure,

Table 2 The interpretation of functionalized GNPs by Fourier-transform infrared spectroscopy

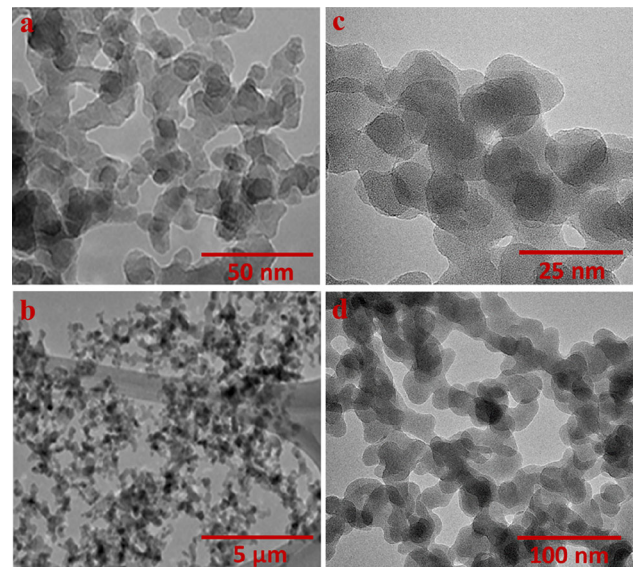
Peak/cm ⁻¹	Interpretation	
919	Stretching vibration (ester band)	C–O
1105	Stretching vibration	C–O
1375	Bending vibration	NH ₂
1463	Bending vibration	CH ₂
1575	Stretching vibration	–C=C
1637	Stretching vibration (ester band)	–C=C
2968 and 2876	Stretching vibration	C–H
3430	O–H and N–H stretching vibration of primary amine/symmetrical –NH stretching vibration	

**Fig. 5** TEM image of functionalized GNP2

which results from the flexibility of GNP flakes after treatment. It is observed that by increasing the wettability of surface, the functionalization can increase the wrinkles.

Characterization of alumina and silicon dioxide

Figure 6 shows the TEM images of 0.1 mass% alumina/water nanofluid. The shape of the alumina nanoparticles is rectangle and rod-like structure (see Fig. 6a). However, Fig. 6b portrays that the sample with 0.1 mass% dispersant has the very minor agglomeration and they reached better suspension. To achieve the better dispersion, alumina nanofluids were sonicated up to 60 min. It can be seen clearly that all particles are of same size and their size is below 50 nm. To achieve the higher TC in alumina nanofluids were prepared without surfactant. Figure 6c represents the TEM images of silica nanoparticles which are round and rod-like in shape. However, Fig. 6d portrays that the samples have the very minor agglomeration and they have reached the better suspension. It can see clearly that all particles are of same size and their size is below 50 nm. To get the stable dispersion, nanofluids were sonicated up to 60 min. In Fig. 6 TEM images, similarly like alumina to achieve the higher TC no surfactant was

**Fig. 6** TEM images of alumina and silicon dioxide at 0.1 mass%

used for silicon dioxide. The majority of the silicon dioxide and alumina indicate good purity of the sample and give confidence in the above-mentioned method of synthesis.

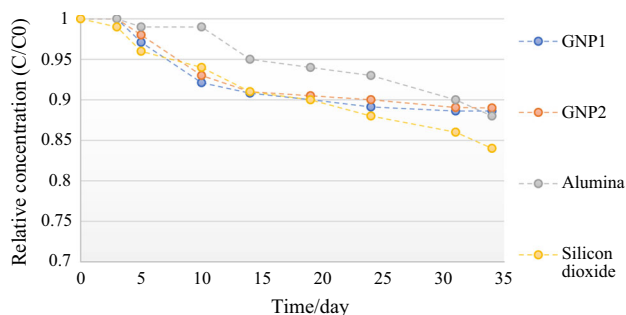
Additionally, zeta potential analysis of the selected samples has carried out the electrophoretic behaviour and useful details to understand the dispersion behaviour of metal oxides in basefluid (water). The analysis of zeta potential and particle size distribution for alumina and silicon dioxide nanofluids is demonstrated in Table 3. It was observed that if the zeta potential has the high complete value, the electrostatic repulsion between particles increases according to the stabilization theory, and then this leads to good stability of suspensions. It is understood that the particles with a high superficial charge always tend not to agglomerate, since contact is contrasting. The zeta potential and the polydispersity index (PDI) of alumina and silicon dioxide at their natural pH are also shown in Table 3. However, the polydispersity index (PDI) and zeta potential are normally applied as an index of magnitude of

Table 3 The particles mobility, zeta potential, size distribution and polydispersity index (PDI) of alumina and silicon dioxide in basefluid (DW)

No.	Sample	Time/day	Avg. particle size distribution/nm	PDI	Zeta potential/mV	Mobility/ $\mu\text{mcm Vs}^{-1}$
1	Alumina	7	138.2	0.192	50.1	3.93
2	Silicon dioxide	7	207.9	0.274	- 35.4	- 2.776

the electrostatic interaction between colloidal particles and hence can be assumed as a measure of colloidal stability of the suspension. Bestowing to Table 3, the zeta potential essential to be as large as possible (negatively or positively) to generate a common repulsive force among the particles. It was observed that after sonication for 1 h alumina is more positively charged, which is around + 50 mV over 7-day period. Similarly, the results of silicon dioxide for zeta potential suggest a suitable stability over 7-day period at 25 °C. Certainly, the zeta potential slowly shows some variations over 7-day period, in spite of mostly remaining stable with the period of time. Measured zeta potential of nanofluids at below - 30 mV or above + 30 mV shows good stability [45, 46]. From the above results, it is suggested that the electrostatic repulsion force between metal oxides is adequate to get over the attraction force among particles. Similarly, it could be observed in Fig. 7 that stability of both alumina and silicon dioxide nanofluids at 0.1 mass% were found stable even after more than a month.

Figure 7 shows the plot of absorbance intensity versus wavelength for the nanomaterials in water taken at a specific period of time (34 days). It depicts the appreciably higher dispersibility of functionalized GNP and metal oxide in aqueous media. The measurement was carried out at a peak wavelength of nanofluids to trace the alteration in the intensity which can be further used to describe the suspension stability at the constant mass fraction of nanomaterials. It can be seen that the colloidal mixture shows a downward trend of relative concentration as the time progressed, indicating that the level of particle concentration and thus the stability subsided. Also, the relative

**Fig. 7** Plot of colloidal stability of selected nanoparticles at 0.1 mass% in distilled water

concentration (absorbance intensity) of tested nanofluids shows the low amount of sediment. The easily miscible PG and TMP functionalities in water may explain the higher dispersion of the functionalized graphite as compared to others.

For GNP1 and GNP2 samples at 0.1 mass%, trend of relative concentration with time, indicating that the level of particle concentration and thus the stability subsided, surprisingly less than 12% sediment. Also, the relative concentration (absorbance intensity) of metal oxides water-based coolant shows the low amount of sediment (maximum of sediment was 12%). However, alumina at 0.1 mass% up to 30 days shows the higher stability among all tested nanofluids. However, in silicon dioxide nanofluid tested at 0.1 mass% the maximum sediment was obtained up to 15% after 34 days.

Uncertainty analysis

The uncertainty analysis was conducted following the conventional paradigm underlined by Kline and McClintock [99] as well as Taylor and Thompson [100] which was established based on the error propagation principle. Both raw and derived parameters were subjected to error analysis to identify the range of uncertainty limit where the true value is likely to exist. Table 4 details the parameters involved within the present uncertainty analysis by which the uncertainty was described in terms of percentage. The

Table 4 Uncertainty analysis conducted for the present work using Kline–McClintock and Taylor and Thompson

Parameter	Error/%
Temperature difference	0.2
Heated section length	2.3
Heat pipe diameter	2
Heat input	3.4
Heat flux	3.2
Thermal resistance	4.2
Heat transfer coefficient	3.6
Nusselt number avg.	5.2
Friction factor	4.9

constitutive expressions elaborating the protocols for calculating these uncertainties were clearly elaborated by Sundar et al. [21]. All the experimental devices are pre-calibrated and the uncertainty results are given in Table 4, with the maximum value listed in each case.

Prior to carrying out the set of detailed experiments on the selected nanofluids, a set of initial experiments were performed for water as the basefluid, in order to assess the accuracy and reliability of the experimental set-up. The empirical correlations of Gnielinsky, Petukhov and Dittus–Boelter [47, 48] were selected for comparison with the obtained results, especially for test of accuracy of the set-up in the turbulent region. The Gnielinski correction is given by Eq. (1) for the range of $3000 < Re < 5 \times 10^6$ and $0.5 < Pr < 2000$. The Petukhov and Dittus–Boelter correlations are given by Eqs. (2) and (3), respectively. The friction factor, f , is given by Eq. (4) as follows (Filonenko [49]):

$$Nu = \frac{\left(\frac{f}{8}\right)(Re - 1000)Pr}{1 + 12.7\left(\frac{f}{8}\right)^{0.5}\left(Pr^{\frac{2}{3}} - 1\right)} \tag{1}$$

$$Nu = \frac{\left(\frac{f}{8}\right)Re Pr}{1 + 12.7\left(\frac{f}{8}\right)^{0.5}\left(Pr^{\frac{2}{3}} - 1\right)} \tag{2}$$

$$Nu = 0.0236 Re^{0.8} Pr^{0.3} \tag{3}$$

$$f = (0.79 \ln Re - 1.69)^{-2} \tag{4}$$

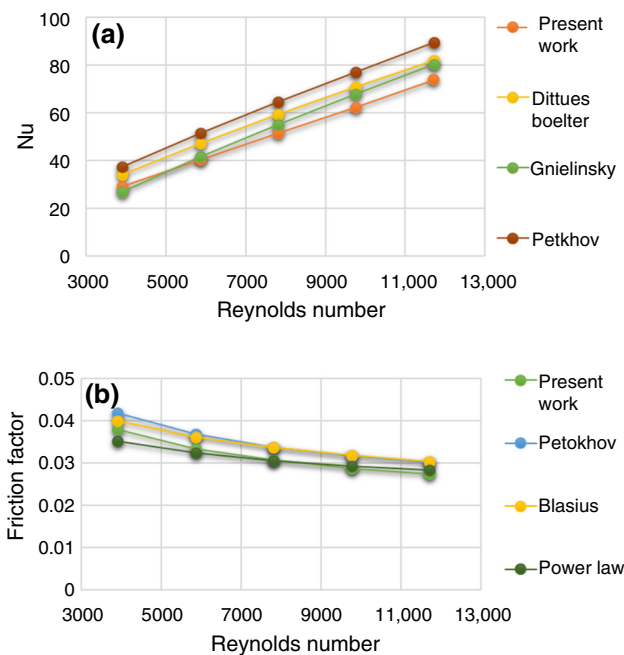


Fig. 8 **a** A comparison of the present heat transfer coefficient data with Gnielinsky, Petukhov and Dittus–Boelter correlations, **b** a comparison of the present friction loss data with Petukhov, Blasius and power law correlations

Figure 8a compares the experimentally measured average Nusselt number for the basefluid at a constant inlet temperature of 30 °C with the empirical correlations. Figure 8 represents the good agreement between the experimental measurements and the Gnielinsky correlation for different Reynolds numbers. For the Nusselt number experiment, the average error was 5.2%, which is quite reasonable. In addition, the correlation of Petukhov and Dittus–Boelter provides a satisfactory agreement with the experimental data for the water. Figure 8a also shows the expected trend of the increase in Nusselt number with Reynolds number. Additionally, for the friction loss the experimental results for basefluid are validated by the Blasius, power law and Petukhov equations. Also, Fig. 8b shows the validation of the friction loss data from the experimental investigation, and the above-mentioned equations are seen to exhibit an error rate of less than 4.9%.

Effect of material on Nu and heat transfer

To investigate the material effect, overheat transfer performance of the nanofluids, three different materials were used for this study which are copper, aluminium and stainless steel with the same diameter of 4 mm, respectively. As the main objective of this study, the copper tube of 4 mm in inner diameter was used to investigate the convective HTC of GNP1, GNP2, alumina and silicon dioxide nanofluids (0.1 mass%) with heat flux of 23,870 W m⁻². Figure 9a presents the convective HTC of all selected samples. However, it shows the HTC, as a function of the nanofluid concentrations at flow velocities of 1–3 m s⁻¹. It can be clearly observed that the enhancement in HTC is increasing by the increase in the velocity, which also shows the good degree of enhancement. It is understood that the increases of the convective HTC of nanofluids significantly surpass those of the TC improvements for different concentration masses. The HTC is increasing by the increase in the velocity of all nanofluids; this proves an enhancement in the heat transfer potential of all the nanofluids as compared to basefluid. Therefore, the highest increment in HTC by using copper tube was achieved up to 119.1% GNP1, 107.59 GNP2, 29.1% alumina and 31.6% silicon dioxide at constant heat flux of 23,870 W m⁻². However, this significant improvement was achieved by adding little number of nanoparticles to the basefluid.

Similarly, to evaluate the convective-to-conductive heat transfer ratio of GNP1, GNP2, alumina and silicon dioxide nanofluids, the averaged Nu of the nanofluids, which is the function of Reynolds number at heat flux of 23,870 W m⁻², is presented in Fig. 9b. Nonetheless, for every case the average Nu of GNP-based and metal oxide

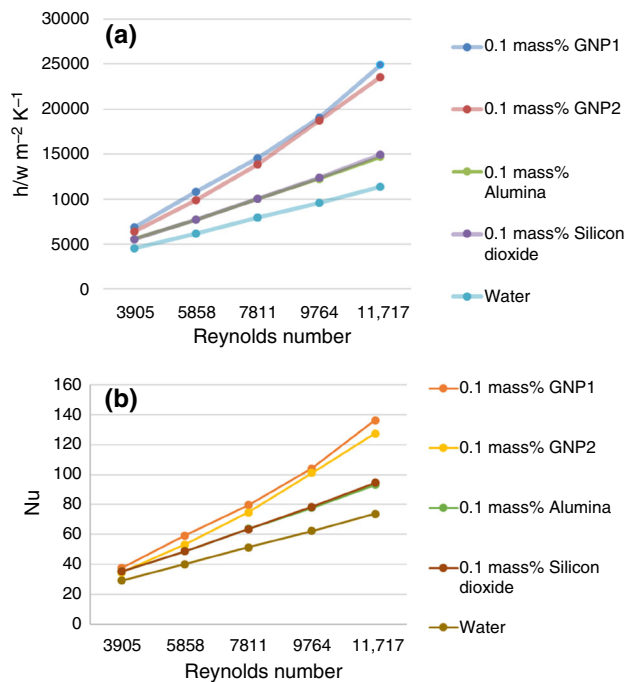


Fig. 9 a Effect of materials and velocity of selected nanofluids on the HTC at input power of $23,870 \text{ W m}^{-2}$ and inlet temperature of $30 \text{ }^\circ\text{C}$, b the average Nu of nanofluids at different velocities with input power of $23,870 \text{ W m}^{-2}$

nanofluids showed significant increment. However, the effect of material and velocity of the GNP2, GNP1, alumina and silicon dioxide nanofluids on Nu were also examined. The maximum Nu of all selected samples was calculated Reynolds number of 1170 and at 0.1 mass% and constant wall heat flux of $23,870 \text{ W m}^{-2}$. The higher Nu for the nanofluid is attributed to the reduction in circulation temperature by the increase in TC of working fluid, which decreases the difference of temperature between the bulk fluid and tube wall in a closed conduit. The maximum increment in Nu of GNP1, GNP2, alumina and silicon dioxide was found up to 82%, 72.5%, 26% and 28% at the heat flux of $23,870 \text{ W m}^{-2}$, respectively.

Similarly, after using the copper tube, the convective HTC of GNP1, GNP2, alumina and silicon dioxide nanofluids with same parameters and concentrations was investigated in aluminium tube of diameter 4 mm. Figure 10a presents the convective HTC of GNP1, GNP2, alumina and silicon dioxide nanofluids. As previously mentioned in copper tube, it shows the HTC as a function of nanofluid concentrations at flow velocities of $1\text{--}3 \text{ m s}^{-1}$. Therefore, clearly the present results reveal the good degree of improvement in convective HTC and this improvement is increased by the increase in velocity. It was observed that the augmentations of the convective HTC of nanofluids significantly exceed beyond those of the TC enhancement for different mass concentrations. In all

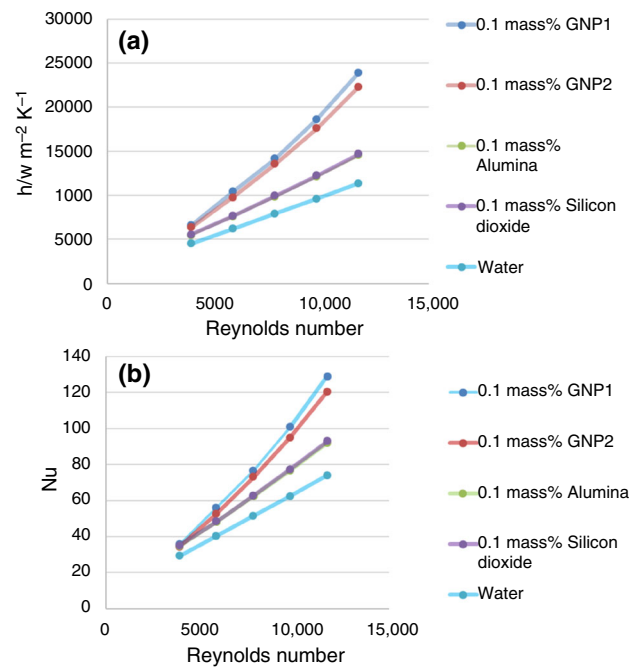


Fig. 10 a Effect of the materials and velocity of nanofluids on the convective HTC (heat flux of $23,870 \text{ W m}^{-2}$), b the average Nu of selected nanofluids at different velocities with input power of $23,870 \text{ W m}^{-2}$

tested nanofluids, the convective HTC is increased by the increase in the velocity, which displays an improvement in the heat transfer potential of the both nanofluids compared to the basefluid. However, in aluminium tube, the maximum increment in HTC of GNP1, GNP2, alumina and silicon dioxide nanofluids at heat flux of $23,870 \text{ W m}^{-2}$ was 110.2%, 96.1%, 27.73% and 29.28%, respectively. This significant enhancement is achieved by adding little number (0.1 mass%) of nanoparticles to the distilled water. By comparing the current results with copper tube, the HTC results are slightly lower in aluminium tube.

Similarly, Nusselt number (Nu) was measured to investigate the convective-to-conductive heat transfer ratio of GNP1, GNP2, alumina and silicon dioxide nanofluids as shown in Fig. 10b. However, Nu of nanofluids which is the function of a Reynolds number was measured at heat flux of $23,870 \text{ W m}^{-2}$. For all of the conditions, the average Nu of the GNP1, GNP2, alumina and silicon dioxide showed good augmentation. However, the effect of material and velocity of the GNP2, GNP1, alumina and silicon dioxide nanofluids on Nu have been noted. The maximum Nu was calculated at Reynolds number of 11,700, heat flux of $23,870 \text{ W m}^{-2}$ and 0.1 mass%. However, the higher Nu for the nanofluid is attributed to the reduction in circulation temperature by the increase in TC of working fluid; this reduces the difference of temperature between the bulk fluid and tube wall in the closed conduit. The highest enhancement in Nu of GNP1, GNP2, alumina and silicon

dioxide was found up to 74.75%, 63%, 24.69% and 25.8%, respectively (heat flux of $23,870 \text{ W m}^{-2}$ and mass percentage of 0.1 mass%), respectively.

In this section, we investigated the convective HTC of GNP1, GNP2 alumina and silicon dioxide nanofluids at heat flux of $23,870 \text{ W m}^{-2}$ and mass percentage of 0.1 mass%. To compare the test section materials effect on heat transfer here, we used the stainless steel tube with diameter of 4 mm. Figure 11a shows the convective HTC of all selected samples. However, it was observed that the as long as the velocity increases, the HTC increases which suggests that the enhancement in HTC is a function of nanofluid concentrations at flow velocities. The obtained results have shown the significant enhancement in convective HTC. Further, the enhancement in heat transfer increases with increasing the velocity. It is observed that the augmentations of the convective HTC of nanofluids significantly go beyond those of the TC enhancements with different mass concentrations. In all tested nanofluids, the convective HTC is increased by the increase in velocity, which shows an improvement in the heat transfer potential of the all test nanofluids compared to basefluid. However, in the stainless steel tube, the maximum enhancement in HTCs of GNP1, GNP2, alumina and silicon dioxide nanofluids at heat flux of $23,870 \text{ W m}^{-2}$ was 100.68%, 93.25%, 26.45% and 28.45%, respectively. It could be proven that the significant enhancement was obtained by adding little amount of nanoparticles to the basefluid. By comparing the stainless steel tube data with the data from

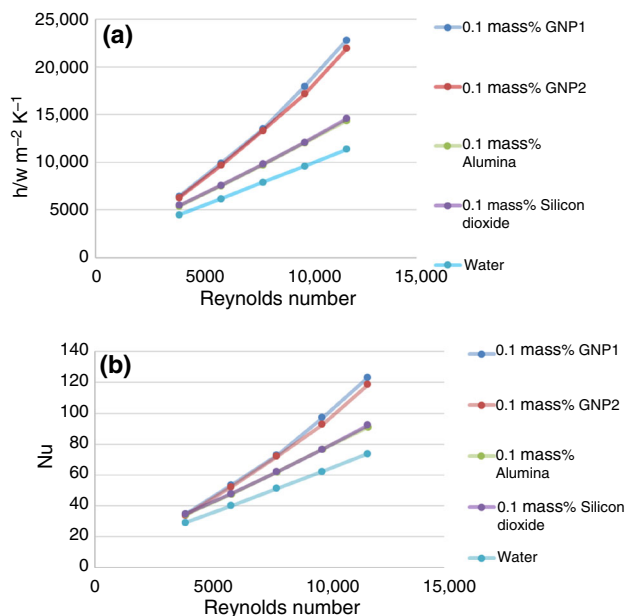


Fig. 11 a Materials effect on the convective HTC of selected nanofluids (heat flux of $23,870 \text{ W m}^{-2}$, b the average Nu of selected nanofluids at different velocities with input power of $23,870 \text{ W m}^{-2}$

aluminium and copper tubes the HTC results are slightly lower in stainless steel tube.

In conclusion, the convective-to-conductive heat transfer ratio of GNP1, GNP2, alumina and silicon dioxide nanofluids was investigated. Figure 11b presents the Nu of the nanofluids which is a function of Reynolds number at heat flux of $23,870 \text{ W m}^{-2}$. Experimentally, in all tested nanofluids the average Nu investigated gave a decent increment. The effect of material and velocity of the GNP1, GNP2, alumina and silicon dioxide nanofluids on Nu have been analysed. The maximum Nu for the nanofluid is attributed to the decrease in circulation temperature by the increment in TC of working fluid, which decreases the difference in temperature between bulk fluid and the tube wall in the closed conduit. The highest increment in Nu of GNP1, GNP2, alumina and silicon dioxide was found up to 66.7%, 60.6%, 23.44% and 25%, respectively, at the heat flux of $23,870 \text{ W m}^{-2}$.

Effect of materials on friction factor

The friction factor of GNP1, GNP2, alumina and silicon dioxide nanofluids flowing through the copper tube was measured under different conditions at various Reynolds number/velocities. Figure 12 shows the measured friction factor of all tested nanofluids, as a function of the flow velocity. It is observed that the friction factor increases with the increase in the percentage of nanofluids, even though some variations were measured in the friction factor at different velocities which were negligible. However, at 0.1 mass% of GNP1 the highest rise in friction factor was measured up to 10.2% at velocities range of $1\text{--}3 \text{ m s}^{-1}$. The friction factor of GNP2 was slightly lower than GNP1 which was measured up to 10%. However, in comparison with the present study, Hooman et al. [36] used the functionalized GNP in squire heat pipe and obtained the enhancement in friction factor up to 9.22% at 0.1 mass% and Re 17,700. However, Emad et al. [11] used GNP

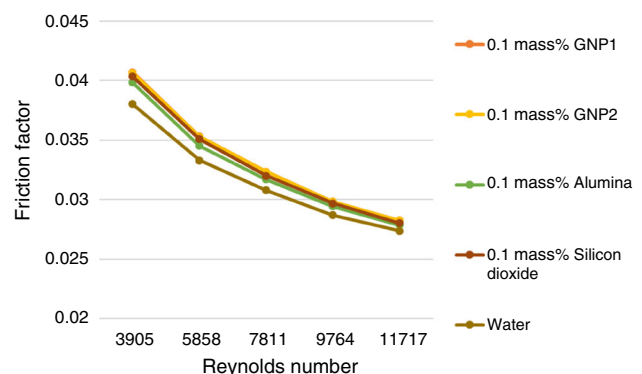


Fig. 12 Friction factor of tested nanofluids in copper tube at different velocities and input power of $23,870 \text{ W m}^{-2}$

nanofluids and obtained the increase in friction factor from 0.4 to 14.3% at 0.1 mass%. Similarly, Sarafraz et al. [27] recorded the 18.3% increase in friction factor at 0.1 mass%. However, in another study Hooman et al. [50] studied the GNP-silver hybrid nanofluids and they achieved the enhancement in friction factor up to 8% at 0.1 mass%. Therefore, it could be understood that the enhancement of the friction factor is due to the suspended GNP nanoparticles in the basefluid which was not significant in comparison with the heat transfer enhancement. For metal oxides, the friction factor of alumina increased up to 5.92% and for silicon dioxide it reached up to 7.14 which is little higher than that of alumina. It could be observed that the dependence of friction factor on nanofluids decreases with the increase in the velocity.

The friction factor of all tested nanofluids in aluminium tube was measured. It was observed that along with the decrease in HTC in aluminium tube compared to copper tube the friction factor for all materials also decreased. The friction factor of GNP1 increased up to 7.88%, and for GNP2 it increased up to 7.21%. Similarly, for alumina, the friction factor increased up to 4.87%, and for silicon dioxide it increased 6.28, respectively (see Fig. 13).

Figure 14 presents the measured friction factor of all materials in stainless 316 tube. The friction factor for GNP1 increased up to 7.08%. Likewise, the friction factor for GNP2 nanofluids increased up to 6.95%. Lastly, for metal oxides, the friction factor for alumina was measured up to 4.74%, while the friction factor of silicon dioxide increased up to 6.1 as a function of the flow velocity. However, it could be observed that the dependence of friction factor on the percentage of alumina decreases with the increase in velocity.

The effect of tube material on convective heat transfer of various nanofluids was measured experimentally. However, in all selected test section materials the HTC dramatically increased in copper tube. This could be the reason that copper material has the highest thermal

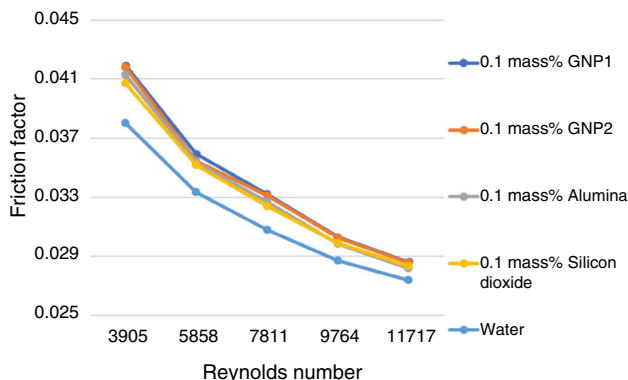


Fig. 13 Friction factor of tested nanofluids in aluminium tube at different velocities and input power of $23,870 \text{ W m}^{-2}$

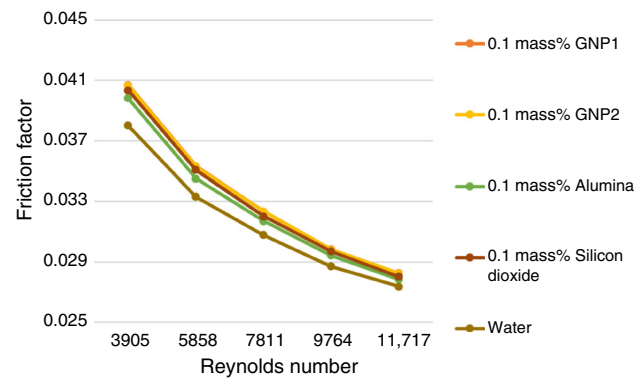


Fig. 14 Friction factor of tested nanofluids in stainless steel tube at different velocities and input power of $23,870 \text{ W m}^{-2}$

conductivity and it is the best conductor of heat. Compared to the aluminium and stainless steel tubes the HTC coefficient of GNP1 at 0.1 mass% increased up to 119% compared to the basefluid which is 18.42% higher than that of aluminium tube and 8.9% higher than that of stainless steel tube measured results (see Fig. 15). The main reason could be the low thermal conductivity of aluminium and stainless steel tube materials. However, HTC of GNP1 nanofluid at 0.1 mass% in aluminium tube was achieved up to 110.2% compared to the basefluid which is 9.1% higher than that of the stainless steel tube results. The heat transfer performance and friction loss results of all tested nanofluids and tubes are presented in Table 5. Previously, it has been discussed that Brownian motion can be the key parameter which affected on the momentum transfer between the basefluid molecules and the nanoparticles at low extent of the Reynolds numbers. Hence, as the Brownian motion increases, in the presence of both types of nanofluids the friction factor increases with the higher slope in comparison with basefluid [51, 52]. Nonetheless, this mechanism is not dominant when there is a high extent of Reynolds number. To summarize this, the key parameter to increase the friction factor at the large extent of Reynolds number can be considered as the velocity of working

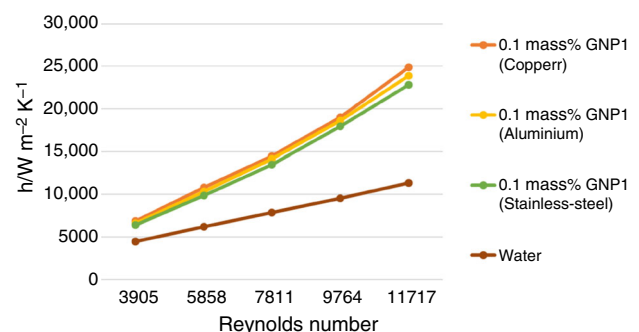


Fig. 15 Effect of tube material on convective heat transfer of various nanofluids

fluid. In general, the slight difference between friction factors of the basefluid in metal oxides and functionalized nanofluids suspension at different volume flow rates is attributed to the insignificant gap between the viscosities of basefluids and nanofluids. The change of friction factor is based on the viscous drag effects of the nanofluids. Therefore, the density of nanoparticle is essential parameter to increase the friction factor of nanofluids. In the flow regime, the pressure drop is directly proportional to the viscosity of fluid. This increment in the viscosity leads to an undesired increase in pumping power. Consequently, the design of a heat exchanger for minimum pumping power and efficient heat transfer is significant in terms of energy savings. The HTC and measured friction factor of selected materials are shown in Table 5.

The heat transfer performance between the basefluid and nanofluids is truly important than the heat transfer estimation, as this issue determines whether the nanofluid should be used instead of the basefluid or not. However, the heat transfer estimation is a crucial parameter which affects the pumping power and heat transfer considerations. This enhancement appears from the TC enhancements. The TC of copper is higher than that of aluminium and stainless steel; therefore, in the result it delivered the higher convective transfer coefficient. By comparing the copper tube with aluminium, the HTC of GNP1, GNP2, alumina and silicon dioxide 8.9%, 11.69%, 1.37% and 2.4%, respectively, was higher than that of aluminium. Similarly, by relating the copper tube with stainless steel, the HTC of GNP1, GNP2, alumina and silicon dioxide 18.42%, 14.34, 2.65 and 3.14% respectively was higher than that of stainless steel tube (see Table 5). It is appeared that GNP1 and GNP2 nanofluids can function as working fluids in heat transfer applications and provide good alternatives to conventional working fluids in the thermal fluid systems. Consequently, it is believed that the GNP1 and GNP2 nanofluids can be brought into the considerations of design engineers and also can be used in many practical engineering applications.

Conclusions

The research experimentally investigated the heat transfer and friction loss characteristics of GNP1, GNP2, alumina and silicon dioxide water-based nanofluids. The convective heat transfer in circular tubes of different materials was used at constant wall heat fluxes of $23,870 \text{ W m}^{-2}$ and nanoparticles concentration of 0.1 mass%. An innovative functionalization approach was used to prepare highly dispersed GNP2- and GNP1-based nanofluids. In the results, the graphene-based samples GNP1 and GNP2 samples showed a significant degree of GNP functionalization with PG and TMP functionality. The measured thermophysical properties of all nanofluids showed significant enhancement which is required for a good heat exchanging liquid. Further, all the selected nanofluids gave significant enhancement in heat transfer characteristics. In the materials effect study, the copper material which is the best conductor of heat that showed the highest heat transfer performance compared to the stainless steel and aluminium tube materials. The remarkable conclusions are listed as follows.

1. Maximum thermal performance enhancement of GNP1, GNP2, alumina and silicon dioxide could be achieved up to 32% and 31%, 7.4% and 9% at 0.1 mass%, respectively.
2. In materials effect, the highest HTC of GNP1 and GNP2 nanofluids was achieved in the copper tube which was measured up to 119% and 107% at heat flux of $23,870 \text{ W m}^{-2}$. However, the purpose of achieving the highest HTC in copper tube could relate to the higher thermal conductivity of the copper material which is the best conductor of heat.
3. The HTC enhancement in GNP1, GNP2, alumina and silicon dioxide nanofluids in copper by comparison with aluminium and stainless steel tubes was higher up to 18.42%, 14.34%, 2.65, 3.14% and 8.9%, 11.69%, 1.37%, 2.4%, respectively.

Table 5 Friction factor and heat transfer performance of the selected nanofluids on different tubes

Nanofluids	Copper material			Aluminium material			Stainless steel material 316		
	Heat trans. Coeff./%	Nu increment/%	Friction factor increase/%	Heat trans. Coeff./%	Nu increment/%	Friction factor increase/%	Heat trans. Coeff./%	Nu increment/%	Friction factor increase/%
GNP1	119.1	84	10.2	110.2	74.74	7.88	100.68	66.78	7.08
GNP2	107.59	72	10	96.1	63	7.21	93.25	60.6	6.95
Alumina	29.1	26	5.92	27.73	24.69	4.87	26.45	23.4	4.74
Silicon dioxide	31.6	28	7.14	29.2	25.8	6.28	28.46	25	6.1

- The enhancement in Nu by using GNP1, GNP2, alumina and silicon dioxide nanofluids increased dramatically and was achieved up to 84%, 72%, 26% and 28%, respectively.
- The friction factor of GNP1 and GNP2 nanofluids was increased from 4 to 10% by comparison with the basefluid. However, alumina and silicon dioxide could achieve increment up to 5.9% and 7.1%, respectively.

Therefore, at a cost of little more frictional pressure drop the good heat transfer enhancement could be obtained. The results suggest that the copper tube which is a good conductor of heat could be used in the heat exchangers and functionalized GNP nanofluids can be used as the heat exchanging fluids in heat transfer applications which could give a significant substitute to traditional working fluids in heat exchangers and in thermal fluid systems.

Parameter	Symbol	Formula
Heat flux	q''	$\frac{VI}{\pi DL}$
Heat transfer coefficient	h	$\frac{q''}{T_w - T_b}$
Nusselt number	Nu	$\frac{hD}{k}$
Friction factor	f	$\frac{\Delta P}{(L/D)(\rho V^2/2)}$
Reynolds number	Re	$\frac{\rho VD}{\mu}$
Prandtl number	Pr	$\frac{\mu C_p}{k}$

Acknowledgements The authors wish to thank Universiti Teknologi Malaysia and Ministry of Higher Education, Malaysia, for their cooperation and assistance throughout this research. Special appreciation goes to the Research Management Centre of UTM for the financial support through the RUG funding QJ130000.2409.04G39 and QJ130000.2509.16H21.

References

- Amani M, Amani P, Bahiraei M, Wongwises S. Prediction of hydrothermal behavior of a non-Newtonian nanofluid in a square channel by modeling of thermophysical properties using neural network. *J Therm Anal Calorim.* 2019;135(2):901–10.
- Animasaun IL, Koriko KS, Adegbe HA, Babatunde RO, Ibraheem N, Sandeep B. Comparative analysis between 36 nm and 47 nm alumina–water nanofluid flows in the presence of Hall effect. *J Therm Anal Calorim.* 2019;135(2):873–86.
- Arya A, Sarafraz MM, Shahmiri S, Madani SAH, Nikkhah V, Nakhjavani SM. Thermal performance analysis of a flat heat pipe working with carbon nanotube–water nanofluid for cooling of a high heat flux heater. *Heat Mass Transf.* 2018;54(4):985–97.
- Ali HM, Ali H, Liaquat H, Bin Maqsood HT, Nadir MA. Experimental investigation of convective heat transfer augmentation for car radiator using ZnO–water nanofluids. *Energy.* 2015;84:317–24.
- Amiri A, Arzani HK, Kazi SN, Chew BT, Badarudin A. Backward-facing step heat transfer of the turbulent regime for functionalized graphene nanoplatelets based water–ethylene glycol nanofluids. *Int J Heat Mass Transf.* 2016;97:538–46.
- Salari E, Peyghambarzadeh M, Sarafraz MM, Hormozi F, Nikkhah V. Thermal behavior of aqueous iron oxide nano-fluid as a coolant on a flat disc heater under the pool boiling condition. *Heat Mass Transf.* 2017;53(1):265–75.
- Ali HM, Arshad W. Thermal performance investigation of staggered and inline pin fin heat sinks using water based rutile and anatase TiO₂ nanofluids. *Energy Convers Manag.* 2015;106:793–803.
- Ali HM, Arshad W. Effect of channel angle of pin-fin heat sink on heat transfer performance using water based graphene nanoplatelets nanofluids. *International Journal of Heat and Mass Transfer.* 2016.
- Ashori A, Menbari S, Bahrami R. Mechanical and thermo-mechanical properties of short carbon fiber reinforced polypropylene composites using exfoliated graphene nanoplatelets coating. *J Ind Eng Chem.* 2016;38:37–42.
- Khosrojerdi S, Vakili M, Yahyaei M, Kalhor K. Thermal conductivity modeling of graphene nanoplatelets/deionized water nanofluid by MLP neural network and theoretical modeling using experimental results. *Int Commun Heat Mass Transf.* 2016;74:11–7.
- Sadeghinezhad E, Togun H, Mehrali M, Sadeghi Nejad P, Tahan Latibari S, Abdulrazzaq T, Kazi SN, Metselaar HSC. An experimental and numerical investigation of heat transfer enhancement for graphene nanoplatelets nanofluids in turbulent flow conditions. *Int J Heat Mass Transf.* 2015;81:41–51.
- Mehrli M, Sadeghinezhad E, Akhiani AR, Tahan Latibari S, Talebian S, Dolatshahi-Pirouz A, Metselaar HSC, Mehrali M. An ecofriendly graphene-based nanofluid for heat transfer applications. *J Clean Prod.* 2016;137:555–66.
- Nikkhah V, Sarafraz MM, Hormozi F. Application of spherical copper oxide (II) water nano-fluid as a potential coolant in a boiling annular heat exchanger. *Chem Biochem Eng Q.* 2015;29(3):405–15.
- Ali HM, Arshad W. Effect of channel angle of pin-fin heat sink on heat transfer performance using water based graphene nanoplatelets nanofluids. *Int J Heat Mass Transf.* 2017;106:465–72.
- Ghozatloo A, Rashidi A, Shariaty-Niassar M. Convective heat transfer enhancement of graphene nanofluids in shell and tube heat exchanger. *Exp Thermal Fluid Sci.* 2014;53:136–41.
- Salari E, Peyghambarzadeh M, Sarafraz MM, Hormozi F. Boiling heat transfer of alumina nano-fluids: role of nanoparticle deposition on the boiling heat transfer coefficient. *Periodica Polytech, Chem Eng.* 2016;60(4):252–8.
- Ali HM, Babar H, Shah TR, Sajid MU, Qasim MA, Javed S. Preparation techniques of TiO₂ nanofluids and challenges: a review. *Appl Sci.* 2018;8(4):587.
- Solangi KH, Amiri A, Luhur MR, Akbari Ghavimi SA, Kazi SN, Badarudin A, Mohd Zubir MN. Experimental investigation of heat transfer performance and frictional loss of functionalized GNP-based water coolant in a closed conduit flow. *RSC Adv.* 2016;6(6):4552–63.
- Iacobazzi F, Milanese M, Colangelo G, Lomascolo M, de Risi A. An explanation of the Al₂O₃ nanofluid thermal conductivity based on the phonon theory of liquid. *Energy.* 2016;116:786–94.
- Betz AR, Attinger D. Can segmented flow enhance heat transfer in microchannel heat sinks? *Int J Heat Mass Transf.* 2010;53(19):3683–91.
- Sarafraz MM, Safaei MR, Tian Z, Goodarzi M, Filho EPB, Arjomandi M. Thermal assessment of nano-particulate graphene-

- water/ethylene glycol (WEG 60:40) nano-suspension in a compact heat exchanger. *Energies*. 2019;12(10):1–17.
22. Arshad W, Ali HM. Graphene nanoplatelets nanofluids thermal and hydrodynamic performance on integral fin heat sink. *Int J Heat Mass Transf*. 2017;107:995–1001.
 23. Hwang SH, Kim BJ, Baek JB, Shin HS, Bae JJ, Lee SY, Park YB. Effects of process parameters and surface treatments of graphene nanoplatelets on the crystallinity and thermomechanical properties of polyamide 6 composite fibers. *Compos B Eng*. 2016;100:220–7.
 24. Sarafraz MM, Hormozi F. Forced convective and nucleate flow boiling heat transfer to alumina nanofluids. *Chem Eng*. 2014;58(1):37–46.
 25. Hafiz MA, Muhammad DA, Musab S, Qazi SS, Ahmed S. Heat transfer enhancement of car radiator using aqua based magnesium oxide nanofluids. *J Therm Sci*. 2015;19:2039–48.
 26. Sarafraz MM, Safaei MR. Diurnal thermal evaluation of an evacuated tube solar collector (ETSC) charged with graphene nanoplatelets-methanol nano-suspension. *Renew Energy*. 2019;142:364–72.
 27. Sarafraz MM, Yang B, Pourmehran O, Arjomandi M, Ghomashchi R. Fluid and heat transfer characteristics of aqueous graphene nanoplatelet (GNP) nanofluid in a microchannel. *Int Commun Heat Mass Transf*. 2019;107:24–33.
 28. Saad AJ, Wajahat A, Hafiz MA. Multiwalled carbon nanotube nanofluid for thermal management of high heat generating computer processor. *Heat Transf Asian Res*. 2013.
 29. Solangi KH, Amiri A, Luhur MR, Ghavimi SAA, Zubir MNM, Kazi SN, Badarudin A. Experimental investigation of the propylene glycol-treated graphene nanoplatelets for the enhancement of closed conduit turbulent convective heat transfer. *Int Commun Heat Mass Transf*. 2016;73:43–53.
 30. Goodarzi M, Kherbeet AS, Afrand M, Sadeghinezhad E, Mehrali M, Zahedi P, Wongwises S, Dahari M. Investigation of heat transfer performance and friction factor of a counter-flow double-pipe heat exchanger using nitrogen-doped, graphene-based nanofluids. *Int Commun Heat Mass Transf*. 2016;76:16–23.
 31. Soheila AAG, Mehran SH, Mohammad HE, Mohammad AS, Fateme FB. Preparation, characterization and biological assessment of polycaprolactone/starch composites for bone tissue engineering applications. *Modares J Med Sci: Pathobiol*. 2012;15:37–48.
 32. Vakili M, Hosseinalipour SM, Delfani S, Khosrojerdi S, Karami M. Experimental investigation of graphene nanoplatelets nanofluid-based volumetric solar collector for domestic hot water systems. *Sol Energy*. 2016;131:119–30.
 33. Sarafraz MM, Hormozi F. Experimental investigation on the pool boiling heat transfer to aqueous multi-walled carbon nanotube nanofluids on the micro-finned surfaces. *Int J Therm Sci*. 2016;100:255–66.
 34. Sajid MU, Ali HM. Recent advances in application of nanofluids in heat transfer devices: a critical review. *Renew Sustain Energy Rev*. 2019;103:556–92.
 35. Solangi KH, Kazi SN, Luhur MR, Badarudin A, Amiri A, Sadri R, Zubir MNM, Gharehkhani S, Teng KH. A comprehensive review of thermo-physical properties and convective heat transfer to nanofluids. *Energy*. 2015;89:1065–86.
 36. Yarmand H, Gharehkhani S, Shirazi SFS, Amiri A, Alehashem MS, Dahari M, Kazi SN. Experimental investigation of thermo-physical properties, convective heat transfer and pressure drop of functionalized graphene nanoplatelets aqueous nanofluid in a square heated pipe. *Energy Convers Manag*. 2016;114:38–49.
 37. Arzani HK, Amiri A, Kazi SN, Chew BT, Badarudin A. Experimental and numerical investigation of thermophysical properties, heat transfer and pressure drop of covalent and noncovalent functionalized graphene nanoplatelet-based water nanofluids in an annular heat exchanger. *Int Commun Heat Mass Transf*. 2015;68:267–75.
 38. Sarafraz MM, Hormozi F, Nikkha V. Thermal performance of a counter-current double pipe heat exchanger working with COOH-CNT/water nanofluids. *Exp Thermal Fluid Sci*. 2016;78:41–9.
 39. Selvam C, Balaji T, Mohan Lal D, Harish S. Convective heat transfer coefficient and pressure drop of water-ethylene glycol mixture with graphene nanoplatelets. *Exp Thermal Fluid Sci*. 2017;80:67–76.
 40. Selvam C, Lal DM, Harish S. Thermal conductivity enhancement of ethylene glycol and water with graphene nanoplatelets. *Thermochim Acta*. 2016;642:32–8.
 41. Xiao YJ, Wang WY, Chen XJ, Lin T, Zhang YT, Yang JH, Wang Y, Zhou ZW. Hybrid network structure and thermal conductive properties in poly(vinylidene fluoride) composites based on carbon nanotubes and graphene nanoplatelets. *Compos A Appl Sci Manuf*. 2016;90:614–25.
 42. Sarafraz MM, Tlili I, Tian Z, Bakouri M, Safaei MR, Goodarzi M. Thermal evaluation of graphene nanoplatelets nanofluid in a fast-responding HP with the potential use in solar systems in smart cities. *Appl Sci*. 2019;9(10):2101.
 43. Loni R, Asli AEA, Ghobadian B, Kasaean AB, Bellos E. Energy and exergy investigation of alumina/oil and silica/oil nanofluids in hemispherical cavity receiver: experimental study. *Energy*. 2018;164:275–87.
 44. Tiwari AK, Ghosh P, Sarkar J. Performance comparison of the plate heat exchanger using different nanofluids. *Exp Thermal Fluid Sci*. 2013;49:141–51.
 45. Sun B, Peng C, Zuo R, Yang D, Li H. Investigation on the flow and convective heat transfer characteristics of nanofluids in the plate heat exchanger. *Exp Thermal Fluid Sci*. 2016;76:75–86.
 46. Leela VV, Suganthi KS, Rajan KS. Convective heat transfer performance of CuO–water nanofluids in U-shaped minitube: potential for improved energy recovery. *Energy Convers Manag*. 2016;118:415–25.
 47. Dittus FW, Boelter LMK. Heat transfer in automobile radiators of the tubular type. *Int Commun Heat Mass Transf*. 1985;12(1):3–22.
 48. Heris SZ, Shokrgozar M, Poorpharhang S, Shanbedi M, Noie SH. Experimental study of heat transfer of a car radiator with CuO/ethylene glycol-water as a coolant. *J Dispers Sci Technol*. 2013;35(5):677–84.
 49. Filonenko GK. Hydraulic resistance in pipes. *Teplotenergetika*. 1954;1(4):40–4 (in Russian).
 50. Yarmand H, Gharehkhani S, Ahmadi G, Shirazi SFS, Baradaran S, Montazer E, Zubir MNM, Alehashem MS, Kazi SN, Dahari M. Graphene nanoplatelets–silver hybrid nanofluids for enhanced heat transfer. *Energy Convers Manag*. 2015;100:419–28.
 51. Shanbedi M, Amiri A, Rashidi S, Heris SZ, Baniadam M. Thermal performance prediction of two-phase closed thermosyphon using adaptive neuro-fuzzy inference system. *Heat Transf Eng*. 2015;36(3):315–24.
 52. Shanbedi M, Heris SZ, Baniadam M, Amiri A, Maghrebi M. Investigation of heat-transfer characterization of EDI-MWCNT/DI-water nanofluid in a two-phase closed thermosyphon. *Ind Eng Chem Res*. 2012;51(3):1423–8.